Original Article

Int J Oral Biol 46:105-110, 2021
pISSN: 1226-7155 • eISSN: 2287-6618
https://doi.org/10.11620/IJOB.2021.46.3.105

International Journal of Oral Biology
IJOB
Check for updates

Physicochemical properties of different phases of titanium dioxide nanoparticles

Vu Phuong Dong and Hoon Yoo*

Department of Pharmacology and Dental Therapeutic, College of Dentistry, Chosun University, Gwangju 61452, Republic of Korea

The physicochemical properties of crystalline titanium dioxide nanoparticles (TiO_2 NPs) were investigated by comparing amorphous ($amTiO_2$), anatase ($aTiO_2$), metaphase of anatase-rutile ($arTiO_2$), and rutile ($rTiO_2$) NPs, which were prepared at various calcination temperatures (100℃, 400℃, 600℃, and 900℃). X-ray diffraction (XRD) and scanning electron microscopy (SEM) analyses confirmed that the phase-transformed TiO_2 had the characteristic features of crystallinity and average size. The surface chemical properties of the crystalline phases were different in the spectral analysis. As anatase transformed to the rutile phase, the band of the hydroxyl group at 3,600–3,100 cm^{-1} decreased gradually, as assessed using Fourier transform infrared spectroscopy (FT-IR). For ultraviolet-visible (UV-Vis) spectra, the maximum absorbance of anatase TiO_2 NPs at 309 nm was blue-shifted to 290 nm at the rutile phase with reduced absorbance. Under the electric field of capillary electrophoresis (CE), TiO_2 NPs in anatase migrated and detected as a broaden peak, whereas the rutile NPs did not. In addition, anatase showed the highest photocatalytic activity in an UV-irradiated dye degradation assay in the following order: $aTiO_2$ > $arTiO_2$ > $rTiO_2$. Overall, the phases of TiO_2 NPs showed characteristic physicochemical properties regarding size, surface chemical properties, UV absorbance, CE migration, and photocatalytic activity.

Keywords: Titanium dioxide nanoparticles, Physicochemical properties, Anatase, Rutile

Introduction

Titanium dioxide (TiO_2) has been used in various fields such as pharmaceuticals and cosmetics [1–4]. More specifically, TiO_2 were used for dye-sensitized solar cells, gas sensors, electrochromic devices, catalyst, light sensitizers, electro chromophores, optoelectronics, and ceramic membrane [1,4,5]. For dental fields, TiO_2 was used for surface modification of implant to reduce the bacterial adhesion [6] and also as an ingredient of toothpaste, dental resin or amalgam to improve the tensile strength and bioactivity [7–10].

Various forms of TiO_2 nanoparticles (NPs) were generated via the temperature-controlled transformation: amorphous – anatase – rutile [11], which requires dehydration and structural rearrangement of the Ti – O lattice at high temperature [12]. This was achieved via two-stage process: amorphous to anatase conversion by dehydration and rearrangement of the Ti – O lattice, and the precipitation of rutile from the solution of the anatase [13,14]. For the thermal stability, the anatase of TiO_2 is at metastable with lower surface energy while the rutile is at stable phase [11,15]. Structurally both anatase and rutile phases have octahedral structure but the crystal units are different from each other with four or two-edge sharing connectivity [12].

Received August 6, 2021; **Revised** August 31, 2021; **Accepted** August 31, 2021
***Correspondence to:** Hoon Yoo, E-mail: hoon_yoo@chosun.ac.kr https://orcid.org/0000-0002-9249-1446

Recent studies showed that TiO_2 has various properties in optical band gap [16], surface charge, and photocatalytic reactivity [17–20] and these were dependent on the phase composition of TiO_2. Thus, understanding the physicochemical properties of individual crystalline phase of TiO_2 is important to extend the application of TiO_2 NPs into the biomedical field. In this study, we prepared the TiO_2 NPs (amorphous, $amTiO_2$; anatase, $anTiO_2$; a mixture of anatase and rutile, $arTiO_2$ and rutile, $ruTiO_2$) with a specific structure and phase composition by using the controlled calcination method. The physicochemical properties of each crystalline phase of TiO_2 NPs were analyzed and compared by using scanning electron microscopy (SEM), X-ray diffraction (XRD), Fourier transform infrared spectroscopy (FT-IR), ultraviolet-visible (UV-Vis) spectroscopy, capillary electrophoresis (CE), and photocatalytic dye degradation assay. Here we present the results that different phases of crystalline TiO_2 have characteristic properties in crystallinity, particle size, surface chemical property, UV absorption, and photocatalytic activity.

Materials and Methods

1. Chemicals

$TiCl_4$ (99.9%), $(NH_4)_2SO_4$, NH_4OH and bromophenol blue (BPB) were purchased by Sigma-Aldrich (St. Louis, MO, USA).

2. Preparation of TiO_2

Various forms of TiO_2 NPs were prepared by the hydrolysis reaction of $TiCl_4$ and calcination process. Briefly, 1 mL of cold $TiCl_4$ was slowly added into the vial containing 10 mL of cold water while vigorously stirring. After 30 minutes, the mixture was refluxed at 100℃ for 2 hours. After cooling to room temperature, the mixture was diluted with 30 mL of $(NH_4)_2SO_4$ (100 mM) and adjusted pH to 7.0 by adding NH_4OH (2.5 M). The particles formed were centrifuged at 12,000 rpm for 10 minutes and washed with distilled water (× 5) to remove excess chlorine and sulfate. Finally, the particles were dried at 100℃ for 12 hours to get $amTiO_2$ and further calcinated at 400, 600, and 900℃ for 2 hours (heating rate of 100℃/h) to produce $aTiO_2$, $arTiO_2$ and $rTiO_2$, respectively.

3. FT-IR and UV-Vis spectroscopy

FT-IR spectrum in the range of 400–4,000 cm^{-1} was measured using a NICOLET 6700 spectrophotometer (Thermo Scientific, Madison, WI, USA). The UV-Vis absorbance was measured by running U-1900 UV-Vis spectrophotometer (Hitachi, Tokyo, Japan). The sample was prepared by suspending TiO_2 NPs in water (0.05 mg/mL) and scanned in the wavelength range of 250 to 550 nm.

4. XRD analysis

XRD patterns were recorded by an X'Pert PRO Alpha-1 diffraction system (PANalytical B.V., Almelo, Netherlands) with Cu Kα method (λ = 1.54056 Å). The diffraction was observed in the range of 20° to 80° with a step size of 0.02° and a dwell time of 1 second. The fraction of crystallinity was estimated from the specific peak intensity. The crystallite size was calculated by using the following equation:

$$D = K\lambda/\beta\cos\theta$$

where D is the crystal size (nm), K is Scherrer's constant (K = 0.89), λ is the X-ray wavelength of Cu Kα radiation (λ = 1.54056 Å), β is the line width of half maximum (radian), θ is the Bragg's diffraction angle.

5. SEM imaging

SEM was performed by S-4800 SEM instrument (Hitachi). The SEM specimens were prepared by loading TiO_2 NPs on the SEM-Stub (2.5 cm) with double-stick conductive carbon tape (TED PELLA Inc., Redding, CA, USA), and sputter-coating with Pt ion in a Polaron system (Quorum Technologies Ltd., East Sussex, UK). SEM imaging was obtained under the accelerating voltage of 15 kV with ultrahigh resolution mode (emission current of 20 μA; scanning time of 40 seconds; working distance of 5 mm).

6. CE analysis

CE analyses were carried out by a P/ACE 5500 system (Beckman Coulter, Brea, CA, USA) using a background electrode (BGE) of 10 mM sodium borate pH 9.1 and a fused-silica capillary (60 cm length, 100 μm inner diameter) (Polymicro Technologies, Phoenix, AZ, USA). Electrophoresis was carried out at constant positive voltage (+20 kV), current (50 ± 2 μA) and temperature (25℃). The sample (0.1 mg/mL of TiO_2), which was suspended in BGE by sonication for 10 minutes,

was injected into capillary by the pressure of 0.5 psi for 3 seconds. The detection was carried out by a photodiode array detector at the wavelength of 319 nm.

7. Dye degradation assay

A 20 mg of TiO_2 NPs was added into 50 mL of BPB (0.05 mM) solution (100 mM of Tris-HCl, pH 8.5) and sonicated for 10 minutes. The suspension was stirred for 30 minutes in the dark. Dye degradation assay was carried out by UV irradiation (wavelength at 366 nm; distance of 30 cm) with 15W G30T8 Hg-LAMP (Sankyo Denki Co., LTD, Kanagawa, Japan). After appropriate period of irradiation, 200 uL of suspension was centrifuged (10 minutes at 12,000 rpm), and then the supernatant was used to determine the absorbance at 595 nm by a Multiskan EX spectrophotometer (Thermo Fisher Scientific, Shanghai, China). The percent dye degradation was calculated as follows:

$$\text{Percent degradation (\%)} = A_t/A_o \times 100$$

where A_o and A_t are the absorbance at 0 min and t min of UV irradiation.

Results

1. SEM images

The phase transformation of amorphous-anatase-rutile was carried out by adjusting the calcination temperature. The calcination at 400℃ or 900℃ for 2 hours generated pure anatase and rutile TiO_2 while the metaphase TiO_2 was formed at 600℃ (Fig. 1). In SEM images, $amTiO_2$ and $aTiO_2$ showed homogeneous shape with estimated particle size at 9 and 13 nm, respectively. On the contrary, TiO_2 of metaphase or rutile phase ($arTiO_2$ and $rTiO_2$) showed large particle size (20 nm for $arTiO_2$ and 50 to 60 nm for $rTiO_2$) with heterogeneous morphology.

2. XRD analysis

XRD patterns of prepared TiO_2 NPs are shown in Fig. 2A. XRD of $amTiO_2$ was in flat-curve with weak peaks, indicating the amorphous state, not crystalline. The phase transformation of amorphous to anatase and anatase to rutile were confirmed by the change of the peak shapes at 25.2 and 27.1 indicating for anatase and rutile phase, respectively. Also estimated particle size by XRD increased as the calcination temperature was raised (Fig. 2B). The relative size of prepared TiO_2 NPs was in the order of $amTiO_2 < aTiO_2 < arTiO_2 < rTiO_2$, which was consistent with the particle size estimated by SEM.

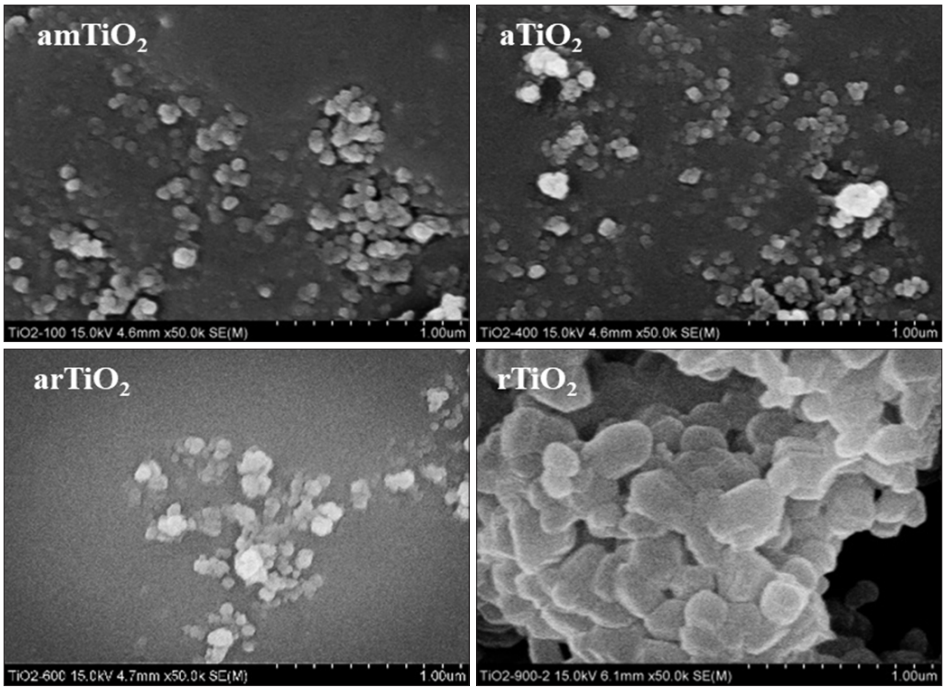

Fig. 1. Scanning electron microscopy images of prepared titanium dioxide (TiO_2) nanoparticles.
$amTiO_2$, amorphous; $aTiO_2$, anatase; $arTiO_2$, metaphase of anatase-rutile; $rTiO_2$, rutile.

3. Surface chemical property

To understand the surface chemical property of prepared TiO_2 NPs, FT-IR spectra were taken (Fig. 3A). All spectra showed the Ti-O-Ti absorption bands at 400–900 cm^{-1} along with stretching bands of Ti-OH at 3,600 – 3,100 cm^{-1} and 1,640 – 1,620 cm^{-1}. However, the peak intensity of hydroxyl group was gradually decreased during the phase transformation of amorphous to anatase and eventually disappeared at rutile phased TiO_2 NPs.

4. UV-Vis spectrum and CE detection

The UV-Vis spectroscopy was used to analyze the surface property of TiO_2 in UV-light absorption. Fig. 3B shows UV-Vis spectra of different crystal types of TiO_2 NPs. The maximum absorbance of $amTiO_2$, $aTiO_2$ and $arTiO_2$ was at 309 nm while $rTiO_2$ was blue-shifted to the wavelength of 290 nm with lower absorbance. Interestingly, $amTiO_2$ had higher maximum absorbance than $aTiO_2$ and $arTiO_2$ with the absorbance order of $amTiO_2$ > $aTiO_2$ > $arTiO_2$ > $rTiO_2$. In the CE electropherogram, $amTiO_2$ and $aTiO_2$ were detected as a broaden peak while $rTiO_2$ was not, suggesting that the surfaces of $amTiO_2$ and $aTiO_2$ are electrically active and physically small enough to migrate in capillary (Fig. 3C).

5. Photocatalytic activity

To further understand the photocatalytic activity of different phases of TiO_2 NPs, the dye degradation assay was carried out by irradiating UV light to organic dye (BPB) solution in the presence of TiO_2 NPs. As shown in the Fig. 4, $aTiO_2$ irradiated with UV light decreased BPB concentration dramatically by the active photocatalytic action while $rTiO_2$ decreased slowly. The relative photocatalytic activity was in the order of $aTiO_2$ > $arTiO_2$ > $rTiO_2$.

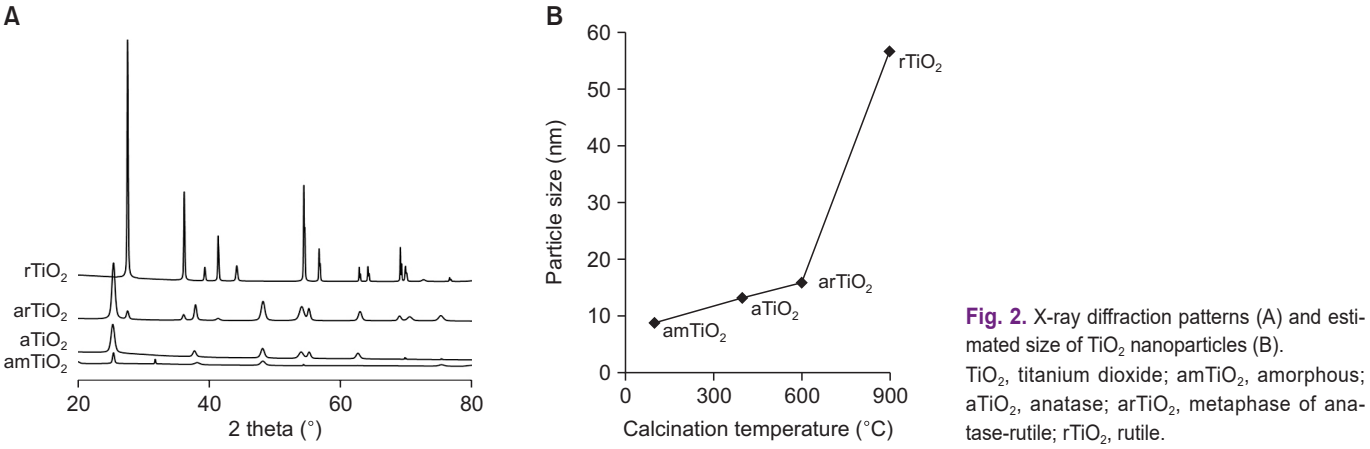

Fig. 2. X-ray diffraction patterns (A) and estimated size of TiO_2 nanoparticles (B).
TiO_2, titanium dioxide; $amTiO_2$, amorphous; $aTiO_2$, anatase; $arTiO_2$, metaphase of anatase-rutile; $rTiO_2$, rutile.

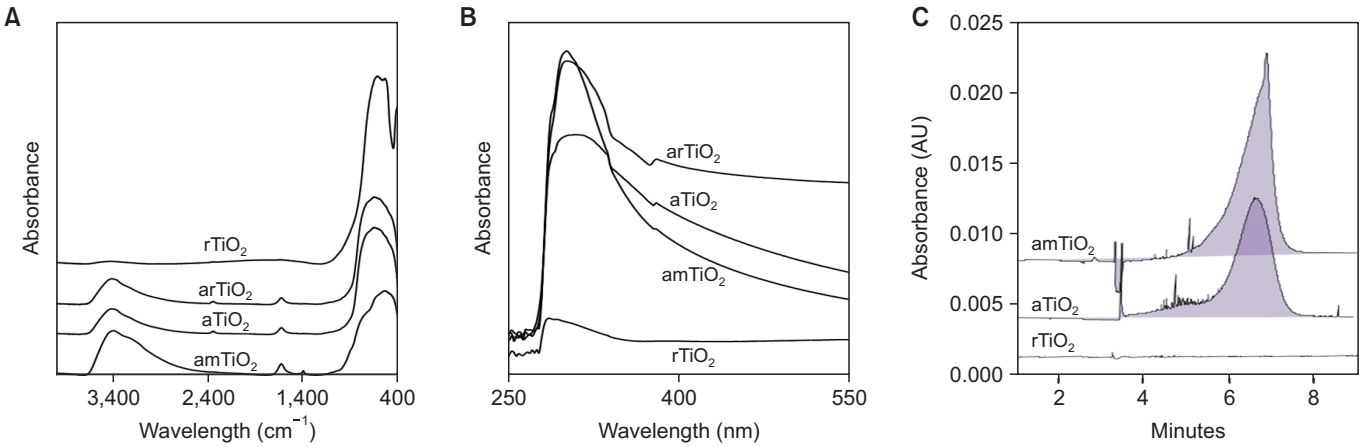

Fig. 3. (A) Fourier transform infrared spectroscopy spectra. (B) Ultraviolet-visible spectra. (C) Capillary electrophoresis electropherogram.
TiO_2, titanium dioxide; $amTiO_2$, amorphous; $aTiO_2$, anatase; $arTiO_2$, metaphase of anatase-rutile; $rTiO_2$, rutile.

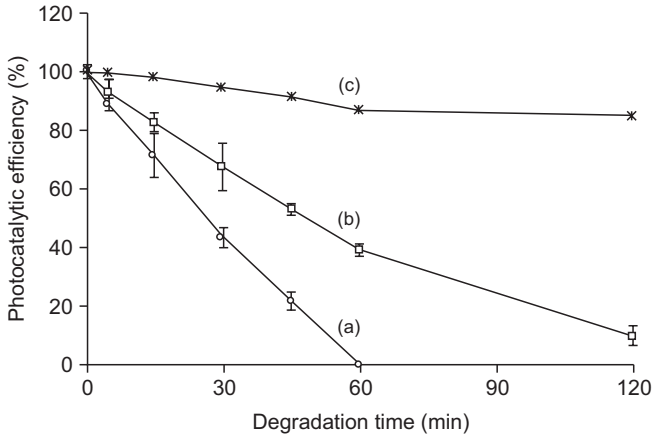

Fig. 4. Dye degradation assay under ultraviolet light irradiation: (a) $aTiO_2$, (b) $arTiO_2$, and (c) $rTiO_2$.
TiO_2, titanium dioxide; $aTiO_2$, anatase; $arTiO_2$, metaphase of anatase-rutile; $rTiO_2$, rutile.

Discussion

In this study, we investigated the physicochemical properties of TiO_2 NPs in different phases ($amTiO_2$, $aTiO_2$, $arTiO_2$, and $rTiO_2$) by analyzing the results of SEM, XRD, FT-IR, UV-Vis spectroscopy, CE, and photocatalytic dye degradation assay. The phase transformations of TiO_2 crystal structure, $amTiO_2$ to $aTiO_2$ and $aTiO_2$ to $rTiO_2$ via the metaphase of $arTiO_2$, were carried out by adjusting the specific calcination temperature. Namely, pure $aTiO_2$, metaphase $arTiO_2$ and pure $rTiO_2$ were prepared by setting specific calcination temperature at 400, 600, and 900℃ for 2 hours. Prepared TiO_2 crystal phases showed characteristic physicochemical properties in particle size, surface chemical property, UV-Vis absorption, CE migration, and photocatalytic activity. In amorphous – anatase – rutile transformation, XRD data revealed the characteristic rearrangement in structure by the changes of peak position, shape, and intensity. In FT-IR spectrum, the surface of $rTiO_2$ was in dehydration with the weak hydroxyl bands at 3,600 – 3,100 cm^{-1} and 1,640 – 1,620 cm^{-1}. The UV absorbance of TiO_2 phase was blue-shifted with the absorbance order of $amTiO_2$ > $aTiO_2$ > $arTiO_2$ > $rTiO_2$. The small sized $aTiO_2$ (13 nm), which would have larger surface area than $rTiO_2$ (57 nm), showed good mobility under the electric field of CE. For $rTiO_2$, surface dehydration and structural rearrangement caused the aggregation of nanoparticles leading to the large-sized heterogeneous shape with different physicochemical properties. The photocatalytic activity of TiO_2 NPs demonstrated that the anatase has the highest catalytic activity with the order of $aTiO_2$ > $arTiO_2$ > $rTiO_2$. The low UV absorbance of $rTiO_2$, probably due to the small surface area, caused poor photocatalytic activity since the small surface generates less reactive species to catalize BPB degradation. Also increased size and poor surface charge of $rTiO_2$ prevented the migration in CE. Overall, we demonstrated that different phases of TiO_2 NPs have characteristic physicochemical properties. Understanding the physicochemical properties of individual crystalline phase of TiO_2 NPs could be important for the future application of TiO_2 NPs in biomedical field.

In conclusion, different phases of TiO_2 NPs ($amTiO_2$, $aTiO_2$, $arTiO_2$, and $ruTiO_2$), generated by the hydrolysis reaction of $TiCl_4$ and calcination at a specific temperature, showed characteristic physicochemical properties in size, shape, surface chemical property, UV-Vis absorption, CE migration, and photocatalytic activity.

Acknowledgements

This study was supported by the research funds from Chosun University, 2019.

Conflicts of Interest

No potential conflict of interest relevant to this article was reported.

References

1. Hashimoto K, Irie H, Fujishima A. TiO_2 photocatalysis: a historical overview and future prospects. Jpn J Appl Phys 2005;44:8269-85. doi: 10.1143/JJAP.44.8269.
2. Bachler G, von Goetz N, Hungerbuhler K. Using physiologically based pharmacokinetic (PBPK) modeling for dietary risk assessment of titanium dioxide (TiO_2) nanoparticles. Nanotoxicology 2015:9:373-80. doi: 10.3109/17435390.2014.940404.
3. Weir A, Westerhoff P, Fabricius L, Hristovski K, von Goetz N. Titanium dioxide nanoparticles in food and personal care products. Environ Sci Technol 2012;46:2242-50. doi: 10.1021/es204168d.
4. Kulkarni M, Mazare A, Gongadze E, Perutkova Š, Kralj-Iglič V, Milošev I, Schmuki P, Iglič A, Mozetič M. Titanium nanostructures for biomedical applications. Nanotechnology 2015;

26:062002. doi: 10.1088/0957-4484/26/6/062002.
5. Waghmode MS, Gunjal AB, Mulla JA, Patil NN, Nawani NN. Studies on the titanium dioxide nanoparticles: biosynthesis, applications and remediation. SN Appl Sci 2019;1:310. doi: 10.1007/s42452-019-0337-3.
6. Almaguer-Flores A, Silva-Bermudez P, Galicia R, Rodil SE. Bacterial adhesion on amorphous and crystalline metal oxide coatings. Mater Sci Eng C Mater Biol Appl 2015;57:88-99. doi: 10.1016/j.msec.2015.07.031.
7. Zhao X, Wang G, Zheng H, Lu Z, Zhong X, Cheng X, Zreiqat H. Delicate refinement of surface nanotopography by adjusting TiO_2 coating chemical composition for enhanced interfacial biocompatibility. ACS Appl Mater Interfaces 2013;5:8203-9. doi: 10.1021/am402319a.
8. Cimpean A, Popescu S, Ciofrangeanu CM, Gleizes AN. Effects of LP-MOCVD prepared TiO_2 thin films on the *in vitro* behavior of gingival fibroblasts. Mater Chem Phys 2011;125:485-92. doi: 10.1016/j.matchemphys.2010.10.028.
9. Shirkavand S, Moslehifard E. Effect of TiO_2 nanoparticles on tensile strength of dental acrylic resins. J Dent Res Dent Clin Dent Prospects 2014;8:197-203. doi: 10.5681/joddd.2014.036.
10. Bahremandi Tolou N, Fathi MH, Monshi A, Mortazavi VS, Shirani F, Mohammadi M. The effect of adding TiO_2 nanoparticles on dental amalgam properties. Iran J Mater Sci Eng 2013;10:46-56.
11. Koparde VN, Cummings PT. Phase transformations during sintering of titania nanoparticles. ACS Nano 2008;2:1620-4. doi: 10.1021/nn800092m.
12. Matthews A. The crystallization of anatase and rutile from amorphous titanium dioxide under hydrothermal conditions. Am Mineral 1976;61:419-24.
13. Khatim O, Amamra M, Chhor K, Bell AMT, Novikov D, Vrel D, Kanaev A. Amorphous–anatase phase transition in single immobilized TiO_2 nanoparticles. Chem Phys Lett 2013;558:53-6. doi: 10.1016/j.cplett.2012.12.019.
14. Hanaor DAH, Sorrell CC. Review of the anatase to rutile phase transformation. J Mater Sci 2011;46:855-74. doi: 10.1007/s10853-010-5113-0.
15. Gouma PI, Mills MJ. Anatase-to-rutile transformation in titania powders. J Am Ceram Soc 2001;84:619-22. doi: 10.1111/j.1151-2916.2001.tb00709.x.
16. Kavan L, Grätzel M, Gilbert SE, Klemenz C, Scheel HJ. Electrochemical and photoelectrochemical investigation of single-crystal anatase. J Am Chem Soc 1996;118:6716-23. doi: 10.1021/ja954172l.
17. Xu M, Gao Y, Moreno EM, Kunst M, Muhler M, Wang Y, Idriss H, Wöll C. Photocatalytic activity of bulk TiO_2 anatase and rutile single crystals using infrared absorption spectroscopy. Phys Rev Lett 2011;106:138302. doi: 10.1103/PhysRevLett.106.138302.
18. Tang H, Prasad K, Sanjinès R, Schmid PE, Lévy F. Electrical and optical properties of TiO_2 anatase thin films. J Appl Phys 1994;75:2042-7. doi: 10.1063/1.356306.
19. Luttrell T, Halpegamage S, Tao J, Kramer A, Sutter E, Batzill M. Why is anatase a better photocatalyst than rutile?--model studies on epitaxial TiO_2 films. Sci Rep 2014;4:4043. doi: 10.1038/srep04043.
20. Liu L, Zhao H, Andino JM, Li Y. Photocatalytic CO_2 reduction with H_2O on TiO_2 nanocrystals: comparison of anatase, rutile, and brookite polymorphs and exploration of surface chemistry. ACS Catal 2012;2:1817-28. doi: 10.1021/cs300273q.